RBF-FD Solution of Electromagnetic Scattering Problem

Blaž Stojanovič[1,2], Jure Slak[1,2], Gregor Kosec[1]

[1] "Jožef Stefan" Institute, Parallel and Distributed Systems Laboratory, Ljubljana, Slovenia
[2] Faculty of Mathematics and Physics, University of Ljubljana, Ljubljana, Slovenia
blaz.stojanovic@student.fmf.uni-lj.si, jure.slak@ijs.si, gregor.kosec@ijs.si

Abstract – In recent years, mesh-free approaches have become a widely used alternative to conventional methods, such as the Finite Element Method, in solving numerical scattering problems. In this work a local Radial Basis Generated-Finite Differences method is used to investigate the electromagnetic scattering problem of an infinitely long anisotropic circular cylinder, described by two coupled complex partial differential equations. The method proves useful for treating the complex valued solutions of the problem with material discontinuity at the junction between the anisotropic cylinder and free space. The numerical solution is compared to a known analytical solution in terms of accuracy and the values of Radar Cross Section.

I. INTRODUCTION

Electromagnetic scattering by different objects has been of interest to physicists for a long time. Mie [1] provided a solution of plane wave scattering by homogeneous dielectric sphere that was later extended to spheroids, ellipsoids [2] and infinite cylinders [3]. In recent decades, motivated by various applications [4, 5, 6], substantial research on electromagnetic scattering by different anisotropic scatterers has been conducted. While closed form solutions for circular [7] and elliptical [8] cylinders exist, it is difficult to find solutions for arbitrary shapes, possibly made of anisotropic materials. This has led to to a wide variety of numerical methods being used to study the problem. Finite-Difference Time-Domain (FD-TD) method, developed by Yee [9], was applied to this problem by Taflove [10] and Umashankar [11], followed by Finite-Difference with Measured Equation of Invariance (FD-MEI) to simulate scattering by a transversely anisotropic cylinder [12, 13]. Also weak form Finite Element Method (FEM) and its variants, namely edge-based FEM, have been widely used to study the problem [14]. Mesh-based methods can however run into problems when solving severely anisotropic problems. Such problems require mesh refinement along the anisotropy direction, which makes them computationally expensive [15].

In the past decades, meshfree or meshless methods based on radial basis functions (RBFs) have emerged as an attractive alternative to the above mentioned mesh-based methods, for solving partial differential equations (PDEs) [16, 17]. The main strength of meshless methods is that there is no need for mesh generation. Furthermore, meshless methods have been applied to a variety of electromagnetic problems [18, 19]. The electromagnetic scattering problem by anisotropic cylinders has been solved using the method of approximate particular solution (MAPS), a global strong form approach [15] and us-ing meshfree local Petrov-Galerkin method (MLPG), a local weak form approach [20].

In this paper Radial Basis Function-generated Finite Differences (RBF-FD), a local strong form approach, is applied to the scattering problem by an anisotropic circular cylinder, the scattering is formulated as a complex valued problem and is solved using in-house Medusa library [21]. The error of the numerical solution is evaluated with respect to the known analytical solution.

The rest of the paper is structured as follows: in section II one can find the formulation of the direct scattering problem from an anisotropic cylinder along with the definition of RCS, RBF-FD method description and details are presented in section III and finally, the numerical solution and its analysis can be found in section IV.

II. ELECTROMAGNETIC SCATTERING PROBLEM

A. Scattering

Let $D \subset \mathbb{R}^2$ be the cross section of an infinitely long anisotropic dielectric cylindrical scatterer surrounded by a free space, with an outward normal n on boundary ∂D. The anisotropy of the scatterer is described by A, a 2×2 symmetric positive definite matrix, whose entries are relative magnetic permeabilities.
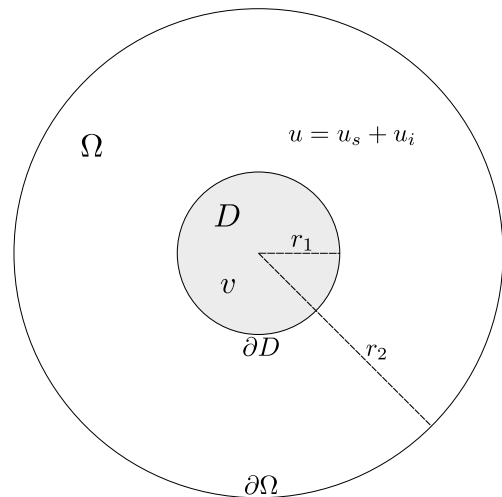
Figure 1. Anisotropic scatterer with cross section D, inside the computational domain Ω.

The scatterer is excited by an $e^{i\omega t}$ time-harmonic plane wave with $\boldsymbol{TM}^z$ polarization, with ω standing for its angular frequency. Let $v \in C^2(\mathbb{C})$ denote the complex

valued field inside the scatterer and $u \in C^2(\mathbb{C})$ the field outside of the scatterer. Field u can be further decomposed into the incident u^i and the scattered field u^s. The scattering of u^i by an inhomogeneity with cross section D in $\mathbb{R}^2$ can be formulated as a system of complex PDEs for v and u:

$$\nabla \cdot A\nabla v + \epsilon_r k^2 v = 0 \qquad \text{in} \quad D \qquad (1)$$

$$\nabla^2 u^s + k^2 u^s = 0 \qquad \text{in} \quad \mathbb{R}^2 \setminus D \qquad (2)$$

with boundary conditions

$$v - u^s = u^i \qquad \text{on} \quad \partial D \qquad (3)$$

$$\frac{\partial v}{\partial n_A} - \frac{\partial u^s}{\partial n} = \frac{\partial u^i}{\partial n} \qquad \text{on} \quad \partial D \qquad (4)$$

$$\lim_{r \to \infty} \sqrt{r}\left(\frac{\partial u^s}{\partial r} - iku^s\right) = 0, \qquad r = |\boldsymbol{r}|, \qquad (5)$$

where $k = \omega\sqrt{\mu_0 \epsilon_0} = \frac{2\pi}{\lambda}$ is the wave number of free space, μ_0 and ϵ_0 are magnetic permeability and electric permittivity of free space, while ϵ_r is the relative electric permittivity of the scatterer. Relative magnetic permeability matrix A is of the following form

$$A = \frac{1}{\mu_{xx}\mu_{yy} - \mu_{xy}^2}\begin{pmatrix} \mu_{xx} & \mu_{xy} \\ \mu_{xy} & \mu_{yy} \end{pmatrix} \qquad (6)$$

and the anisotropic normal derivative is calculated as

$$\frac{\partial v}{\partial n_A} = n \cdot A\nabla v. \qquad (7)$$

To numerically solve the described problem we construct a finite computational domain Ω around our scatterer, as seen on Figure 1. This slightly changes the problem formulation, (2) is now only solved in $\Omega \setminus D$ and (5) changes to:

$$\frac{\partial u^s}{\partial n} + \left(ik + \frac{1}{2r_2}\right)u^s = 0 \quad \text{on} \quad \partial\Omega. \qquad (8)$$

The condition described in (5), and numerically calculated as (8) is the so called Sommerfeld boundary condition and it ensures that the scattered field u^s is outgoing.

B. Radar Cross Section

Radar cross section $\chi(\theta)$, sometimes called the scattering cross section, is often of primary interest rather than the fields u and v themselves, as it can be effectively measured [22]. In 2D it is defined as the following limit:

$$\chi(\theta) = \lim_{r \to \infty} 2\pi r \frac{|\boldsymbol{E}_s(\theta, r)|^2}{|\boldsymbol{E}_i(\theta, r)|^2} = \lim_{r \to \infty} 2\pi r \frac{|\boldsymbol{H}_s(\theta, r)|^2}{|\boldsymbol{H}_i(\theta, r)|^2}, \qquad (9)$$

where $\boldsymbol{E}_s$, $\boldsymbol{H}_s$ and $\boldsymbol{E}_i$, $\boldsymbol{H}_i$ are the far field scattered and incident electric and magnetic field intensities, respectively. For $\boldsymbol{TE}^z$ and $\boldsymbol{TM}^z$, where $|u^i| = 1$, the expression can be further simplified to

$$\chi(\theta) = \lim_{r \to \infty} 2\pi r|u^s(\theta, r)|^2. \qquad (10)$$

Finally given $|u^s|$ along the outer contour we can calculate RCS by expanding the solution in terms of Green's functions for the Helmholtz equation [23].
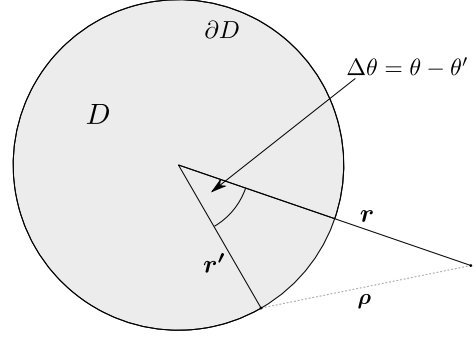
Figure 2. Given $|u^s|$ inside a finite domain, one can calculate the scattered field for any point $\boldsymbol{r}$ outside the domain via Green's function for the Helmholtz equation.

In the case of a circular outer contour the expression simplifies into:

$$\chi(\theta) = \frac{R^2}{4k}\left|\int_0^{2\pi} F[u_s(\boldsymbol{r}')]e^{ikR\cos\Delta\theta}d\theta'\right|, \qquad (11)$$

where R is the radius of the outer contour and

$$F[u_s(\boldsymbol{r}')] = \frac{\partial u_s(\boldsymbol{r}')}{\partial n} - (ik\cos\Delta\theta)u_s(\boldsymbol{r}'), \qquad (12)$$

where $\Delta\theta$ is defined as the angle between vectors $\boldsymbol{r}'$ and $\boldsymbol{r}$ as depicted in Figure 2. We will use the $|u^s|$ calculated in the points on the boundary ∂D, as they are most densely spaced in angle θ. Hence R in the above equations is really r_1.

III. NUMERICAL METHOD

A. Radal basis functions

The foundation of the RBF-FD method are radial basis functions. They are defined over a set of nodes $X = \{x_1, \ldots x_n\}$ generated by a radial function $\phi \colon [0, \infty) \to \mathbb{R}$ as

$$\{\phi_i := \phi(\| \cdot -x_i\|), \text{ for } x_i \in X\}. \qquad (13)$$

Commonly used RBFs are Gaussians, which we will also be using in this paper. They are defined as

$$\phi_i(x) = \exp(-(\varepsilon r)^2), \qquad (14)$$

where $r = \|x - x_i\|$ and ε is the shape parameter which controls the flatness of radial basis functions.

B. Solution procedure

A discrete formulation of a PDE is obtained by using the RBF-FD method. Consider an elliptic boundary value problem with Dirichlet boundary conditions

$$\mathcal{L}u = f \qquad \text{in} \quad \Omega \qquad (15)$$

$$u = u_0 \qquad \text{on} \quad \partial\Omega, \qquad (16)$$

where f and u_0 are known functions. In order to obtain a discrete representation of the PDE, the domain is populated with N nodes. N_i nodes are placed in the interior of the domain and N_b on its boundary. Each node x_i is

assigned n neighbors, denoted $N(x_i)$, that constitute its *support domain* or *neighborhood*.

RBD-FD is a natural generalization of the FD method. When using the FD method, stencil weights for operator $\mathcal{L}$ are known in advance. For example, if $\mathcal{L}$ is the second derivative on a one dimensional equispaced grid with spacing h, the weights are $[1/h^2, -2/h^2, 1/h^2]$. Assembling the weights gives a global sparse system, whose solution is an approximation of u in points x_i. RBF-FD works the same way, except the stencil weights cannot be known in advance, as different neighborhoods have different arrangements, hence computing the weights becomes a part of the solution procedure. Moreover the operator $\mathcal{L}$ is approximated as a linear combination of function values at support points

$$(\mathcal{L}u)(x_i) \approx \sum_{x_j \in N(x_i)} w_j^i u(x_j). \qquad (17)$$

Weights w_j^i are computed by imposing exactness of (17) for a set of radial basis functions, as it is done with monomials in the FD method. This gives a set of equations

$$(\mathcal{L}\phi_k)(x_i) = \sum_{x_j \in N(x_i)} w_j^i \phi_k(x_j), \qquad (18)$$

for all $x_k \in N(x_i)$. Rewriting (18) in matrix form, one obtains

$$\begin{bmatrix} \phi(r_{j_1}^{j_1}) \cdots \phi(r_{j_1}^{j_n}) \\ \vdots \ddots \vdots \\ \phi(r_{j_n}^{j_1}) \cdots \phi(r_{j_n}^{j_n}) \end{bmatrix} \begin{bmatrix} w_{j_1}^i \\ \vdots \\ w_{j_n}^i \end{bmatrix} = \begin{bmatrix} (\mathcal{L}\phi_{j_1})(x_i) \\ \vdots \\ (\mathcal{L}\phi_{j_n})(x_i) \end{bmatrix}, \qquad (19)$$

where $r_{j_m}^{j_k} = \|x_{j_k} - x_{j_m}\|$ and j_k are indices of nodes in the neighborhood $N(x_i)$ of node x_i. This is a system of n linear equations and can be compactly written as $A_i w_i = b_i$. Matrix A_i is symmetric and in the case of Gaussian basis functions with distinct support nodes [24], positive definite, hence nonsingular.

After the weight vectors w_i for all nodes n are computed, they are assembled in a sparse matrix, and f and x_0 are used to obtain the right hand side of the system. The system is then solved to give an approximation of u. Boundary conditions that include differential operators, such as Neumann (4) or Sommerfield (8) boundary conditions, are discretized using RBF-FD analogously to operator $\mathcal{L}$.

C. Remarks on weight computation

It should be noted that the value of the shape parameter ε is important as it influences the performance of the algorithm. It is known for example, that as ε decreases, the accuracy of the solution increases, but the matrices A_i become more and more ill conditioned [25]. This is combated by scaling the shape parameter ε inversely proportional to the internodal distance, as this keeps the condition number of A_i constant with increasing node density. For large values of ε and variable nodal densities, issues may arise due to the Runge phenomenon [26]. The authors used the scaling shape parameter technique and no such issues were detected.

IV. SOLUTION

A. Case description

The scattering of interest is such, that the wavelength of the incident wave is of the same order of magnitude as the scatterer radius. Hence the product of the wave vector k and the radius of the scatterer r_1 characterizes the problem. We will be studying incident plane wave that is $\boldsymbol{TM}^z$ polarized, with linear frequency of $300\,\mathrm{MHz}$ and of the form

$$u^i = \exp(ik(x\cos\theta^i + y\sin\theta^i)), \qquad (20)$$

where θ^i is the angle of the incident wave. To get the radius of the scatterer we set $kr_1 = \frac{\pi}{2}$, to obtain $r_1 = 0.25$. As it is customary [15, 20], we chose the radius of the outer computational domain to be three times that of the inner boundary. The authors also solved the problem with different ratios in the range $\frac{r_2}{r_1} \in [2, 15]$ and larger ratios provided no additional accuracy when computing RCS and were much more computationally expensive, while $\frac{r_2}{r_1} = 2$ was unstable. Finally, the relative permeability matrix of our problem is

$$A = \frac{1}{16} \begin{pmatrix} 5 & 3 \\ 3 & 5 \end{pmatrix} \qquad (21)$$

the incident angle $\theta^i = \frac{\pi}{4}$ and the electric permittivity of the scatterer is $\epsilon_r = 0.5$.

B. Numerical solution

The problem was solved using the RBF-FD method described in section III. Gaussian basis functions $\phi_i(x) = \exp(-(\varepsilon r)^2)$ were used, with a support size of $n = 9$. The value of the shape parameter ε was set to $\varepsilon \approx 0.0011$. Both the field inside the scatterer and the scattered field are calculated simultaneously as they are coupled via the nodes they share on the boundary of the cylinder. A common way to solve complex valued problems is to decompose the system of equations into real and imaginary parts and obtain a new system of coupled equations. The medusa library [21], can however solve complex valued problems natively, simplifying the process. While both the real and the complex part of the scattered field are needed to calculate the radar cross section the magnitude of the field inside the scatterer and the magnitude of the scattered field are shown in Figures 3 and 4
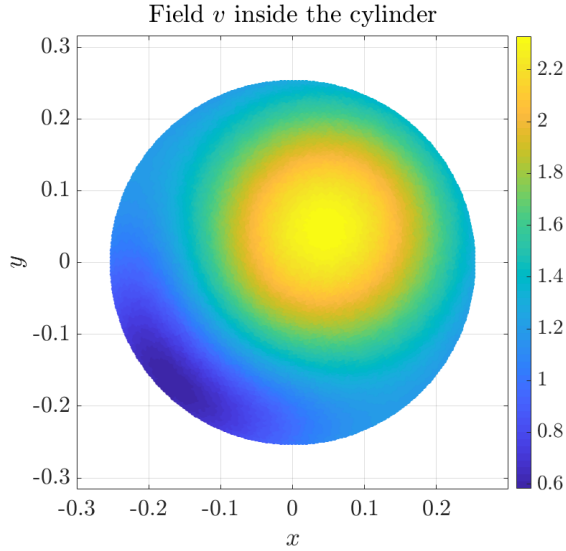
Figure 3. Magnitude of the field inside the cylinder. Number of computational nodes $N_i = 6986$.
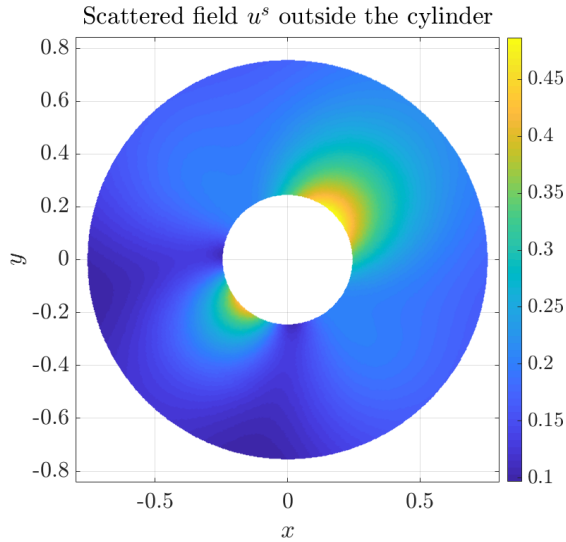
Figure 4. Magnitude of the scattered field outside the cylinder. Number of computational nodes $N_i = 55262$.

Note, the discontinuity at the boundary between the cylinder and free space, which is a result of plotting only the scattered field outside the cylinder. The sum of the incident and the scattered produces a continuous field. The numerical solution is compared to the analytical solution derived by Monzon [27].

To compare the analytical and numerical solution we computed the average error, defined as

$$\varepsilon_{\mathrm{a}} = \frac{1}{N} \sum_{i=1}^{N} |\hat{u}_i - u_i| \tag{22}$$

where, $\hat{u}_i$ and u_i are the analytical and numerical solution in i-th node respectively. Since the numerical solution is sensitive to node distributions, the error was computed for 120 slightly different nodal arrangements and then averaged out. This was repeated for different number of nodes N inside the domain. The results are presented in Figure 5 and Figure 6.
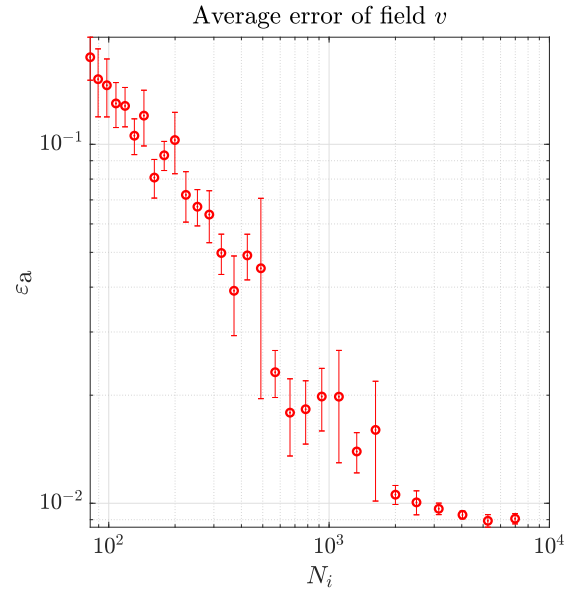
Figure 5. Average error of the numerically calculated field v inside the scatterer, with regards to the number of nodes inside the scatterer N_i.
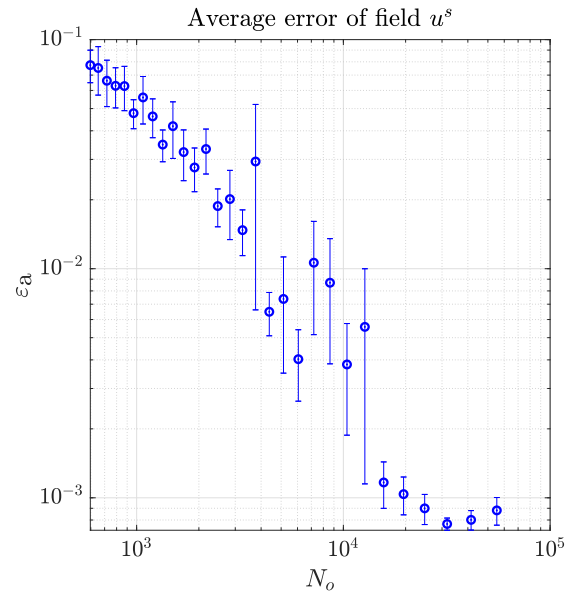
Figure 6. Average error of the numerically calculated field u^s outside the scatterer, with regards to the number of nodes outside the scatterer N_o.

The errorbars in figures 5 and 6 represent the standard error of the mean

$$\sigma_x = \frac{\sigma}{\sqrt{N}} \tag{23}$$

σ being the standard deviation.

C. Radar Cross Section

The radar cross section is obtained from the numerically scattered field by using (11). Normal derivatives of the scattered field are needed for the computation of RCS and they are obtained by explicitly taking the gradient of the computed scattered field u^s using the RBF-FD method. With that, calculating the radar cross section becomes a matter of correctly applying numerical integration techniques; interpolants of both the values and the

normal derivatives of the scattered field are constructed, and then used to numerically integrate (11). The results for the considered case are shown in Figure 7.
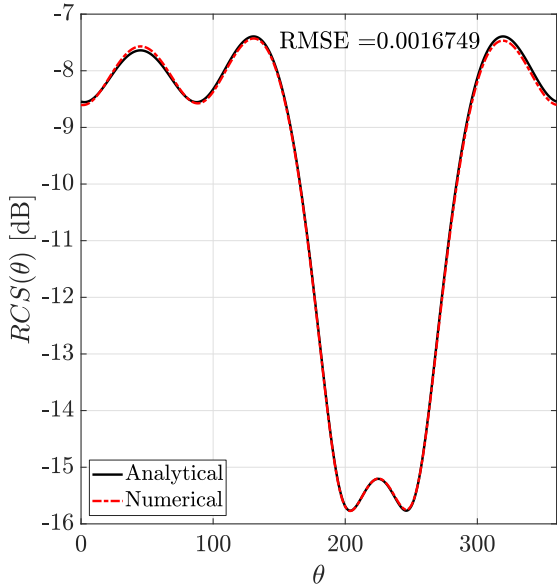
Figure 7. Radar cross section for $\epsilon_r = 0.5$, $\mu_{xx} = \mu_{yy} = 5$, $\mu_{xy} = \mu_{yx} = 3$, $\theta^i = \frac{\pi}{4}$ and $kr_1 = \pi/2$.

The analytical solution shown in Figure 7 was calculated using the method described in [27]. The root mean square error (RMSE), defined as

$$\text{RMSE} = \sqrt{\frac{1}{N_{\text{rcs}}} \sum_{i=1}^{N_{\text{rcs}}} [\hat{\chi}(\theta) - \chi(\theta)]^2} \qquad (24)$$

where $\hat{\chi}$ and χ are the analytical and numerical RCS respectively and N_{rcs} is the number of points in which RCS was calculated. For this case we obtain that RMSE = $1.6749 \cdot 10^{-3}$.

V. Conclusion

In this paper we present a solution to the direct scattering problem by an infinitely long anisotropic cylinder using the RBF-FD method. It was shown that the method gives satisfactory results when compared to the analytical solution of the problem, both in terms of field strength and RCS. Thus showing that RBF-FD method is a good alternative to other meshless methods (MAPS, MLPG) when applied to the scattering problem.

In future work the solution will be extended to irregularly shaped domains in three dimensions with application of refinement of nodes distribution.

References

[1] Gustav Mie. Beiträge zur optik trüber medien, speziell kolloidaler metallösungen. *Annalen der physik*, 330(3):377–445, 1908.

[2] Paul Latimer. Light scattering by ellipsoids. *Journal of Colloid and Interface Science*, 53(1):102–109, 1975.

[3] Milton Kerker. *The scattering of light and other electromagnetic radiation: physical chemistry: a series of monographs*, volume 16. Academic press, 2013.

[4] Victor N. S. Bong and Basil T. Wong. A study of phonon anisotropic scattering effect on silicon thermal conductivity at nanoscale. In *AIP Conference Proceedings*, volume 1674, page 020016. AIP Publishing, 2015.

[5] Adnan H. Nayfeh and Michael J. Anderson. Wave propagation in layered anisotropic media with applications to composites, 2000.

[6] S. V. Nghiem, R. Kwok, Jin Au Kong, and R. T. Shin. A model with ellipsoidal scatterers for polarimetric remote sensing of anisotropic layered media. *Radio science*, 28(5):687–703, 1993.

[7] Xin Bao Wu and Kiyotoshi Yasumoto. Three-dimensional scattering by an infinite homogeneous anisotropic circular cylinder: an analytical solution. *Journal of applied physics*, 82(5):1996–2003, 1997.

[8] Abdul-Kadir Hamid and Francis R. Cooray. Scattering of a plane wave by a homogeneous anisotropic elliptic cylinder. *IEEE Transactions on Antennas and Propagation*, 63(8):3579–3587, 2015.

[9] Kane Yee. Numerical solution of initial boundary value problems involving maxwell's equations in isotropic media. *IEEE Transactions on antennas and propagation*, 14(3):302–307, 1966.

[10] Allen Taflove and Morris E. Brodwin. Numerical solution of steady-state electromagnetic scattering problems using the time-dependent maxwell's equations. *IEEE transactions on microwave theory and techniques*, 23(8):623–630, 1975.

[11] Korada Umashankar and Allen Taflove. A novel method to analyze electromagnetic scattering of complex objects. *IEEE transactions on electromagnetic compatibility*, (4):397–405, 1982.

[12] Zhi Ning Chen, Wei Hong, and Wen Xun Zhang. Application of fd-mei to electromagnetic scattering from transversally anisotropic inhomogeneous cylinders. *IEEE transactions on electromagnetic compatibility*, 40(2):103–110, 1998.

[13] Benjamin Beker and Korada Umashankar. Analysis of electromagnetic scattering by arbitrarily shaped two-dimensional anisotropic objects: combined field surface integral equation formulation. *Electromagnetics*, 9(2):215–229, 1989.

[14] Weimin Sun and Constantine A. Balanis. Edge-based FEM solution of scattering from inhomogeneous and anisotropic objects. *IEEE transactions on antennas and propagation*, 42(5):627–632, 1994.

[15] Maryam Hajisadeghi Esfahani, Hadi Roohani Ghehsareh, and Seyed Kamal Etesami. The extended method of approximate particular solutions to simulate two-dimensional electromagnetic scattering from arbitrary shaped anisotropic objects. *Engineering Analysis with Boundary Elements*, 82:91–97, 2017.

[16] Gregor Kosec and Božidar Šarler. Solution of thermo-fluid problems by collocation with local pressure correction. *International Journal of Numerical Methods for Heat & Fluid Flow*, 18(7/8):868–882, 2008.

[17] Jure Slak and Gregor Kosec. Adaptive rbf-fd method for contact problems. *arXiv preprint arXiv:1811.10368*, 2018.

[18] Y Marchal. Some meshless methods for electromagnetic field computation. *IEEE Trans. Magn.*, 34(5):3351–3354, 1998.

[19] SL Ho, Shiyou Yang, José Márcio Machado, and Ho-ching Chris Wong. Application of a meshless method in electromagnetics. *IEEE transactions on magnetics*, 37(5):3198–3202, 2001.

[20] Maryam Hajisadeghi Esfahani, Hadi Roohani Ghehsareh, and Seyed Kamal Etesami. A meshless method for the investigation of electromagnetic scattering from arbitrary shaped anisotropic cylindrical objects. *Journal of Electromagnetic Waves and Applications*, 31(5):477–494, 2017.

[21] Jure Slak and Gregor Kosec. Parallel coordinate free implementation of local meshless method. In *2018 41st International Convention on Information and Communication Technology, Electronics and Microelectronics (MIPRO)*, pages 0172–0178. IEEE, 2018.

[22] Robert B Dybdal. Radar cross section measurements. *Proceedings of the IEEE*, 75(4):498–516, 1987.

[23] Michael A Morgan. Principles of finite methods in electromagnetic scattering. In *Finite Element and Finite Difference Methods in Electromagnetic Scattering*, pages 1–68. Elsevier, 1990.

[24] Bengt Fornberg and Natasha Flyer. Solving pdes with radial basis functions. *Acta Numerica*, 24:215–258, 2015.

[25] Bengt Fornberg, Erik Lehto, and Collin Powell. Stable calculation of gaussian-based rbf-fd stencils. *Computers & Mathematics with Applications*, 65(4):627–637, 2013.

[26] Victor Bayona, Natasha Flyer, Bengt Fornberg, and Gregory A Barnett. On the role of polynomials in rbf-fd approximations: Ii. numerical solution of elliptic pdes. *Journal of Computational Physics*, 332:257–273, 2017.

[27] J. CESAR Monzon and NICKANDERJ Damaskos. Two-dimensional scattering by a homogeneous anisotropic rod. *IEEE Transactions on Antennas and Propagation*, 34(10):1243–1249, 1986.